Supporting Information

Photoconversion of Ag_{31} to Ag_{42} Initiated by Solvated Electrons

Arijit Jana[a], Wakeel Ahmed Dar[a], Sourav Kanti Jana[a], Ajay Kumar Poonia[b], Vivek Yadav[a], Jayoti Roy[a], Sourov Chandra[c], Kumaran Nair Valsala Devi Adarsh[b]*, Robin H. A. Ras[c]*, Thalappil Pradeep[a]*

[a] DST Unit of Nanoscience (DST UNS) and Thematic Unit of Excellence (TUE), Department of Chemistry, Indian Institute of Technology Madras, Chennai – 600036, India

[b] Department of Physics, Indian Institute of Science Education and Research Bhopal, Bhopal – 462066, India

[c] Department of Applied Physics, Aalto University, School of Science, Puumiehenkuja 2, 02150, Espoo, Finland

Table of contents

Instrumentation

UV-vis absorption spectroscopy: UV-vis absorption spectra were measured in transmission mode using Perkin Elmer Lambda 365 UV-vis spectrometer using a bandpass filter of 1 nm.

Photoluminescence spectroscopy: Photoluminescence spectra were measured using a Jobin Yvon Nanolog fluorescence spectrometer using a slit width of 3 nm and a resolution bandwidth of 5 nm. The Nanolog instrument has a 450 W xenon-arc lamp source, double monochromator with kinetic gratings, associated reflective optics, and CCD detector. Samples were dissolved in DCM (~3 ml) was placed in a 1 cm quartz cuvette to measure the spectrum.

Scanning transmission electron microscopy: STEM images of Ag_{31} nanocluster were captured using a double Cs-corrected JEM-2200FS transmission electron microscope. The measurement was performed at an accelerating voltage of 200 kV. The sample was prepared by drop-casting Ag_{31} cluster in DCM over the ultrathin carbon-coated copper grid.

Transmission electron microscopy: TEM imaging of Ag_{42} nanocluster was performed using a JEOL 3010 high resolution transmission electron microscope operated at 200 kV. A Gatan multistage CCD camera was used to record the micrograph.

Mass spectrometry: Mass spectra of all the clusters were measured using Waters Synapt G2Si HDMS instrument. The instrument is equipped with an electrospray ionization source, mass-selected ion trap, ion mobility cells, and time of flight mass analyzer. An optimized operating conditions such as flow rate 15-20 μL/min, capillary voltage 2-3 kV, cone voltage 20 V, source offset 10 V, desolvation gas flow 400 L/min and source temperature 80-100 °C were used for the measurements. Collision-induced dissociation (CID) studies were performed upon colliding the selected molecular ion with argon gas inside the trap cell of the instrument. Gradually increasing the collision energy (CE 0 to 70 for Ag_{31} and CE 0 to 150 for Ag_{42}) leads to the fragmentation of the species. All the measurements used low concentrations (~ 1 μg/ml) of cluster samples.

Infrared spectroscopy: FT-IR spectra were measured using a JASCO-4100 FT-IR spectrometer after preparing potassium bromide (KBr) pallets of the respective samples.

X-ray photoelectron spectroscopy: XPS data were measured using an ESCA probe TPD equipped with a polychromatic Mg Kα X-ray source (hν = 1253.6 eV). The binding energy of the spectral regions of different elements was calibrated with respect to C 1s (285.0 eV).

NMR spectroscopy: NMR spectra were measured using a Bruker 500 MHz NMR instrument. Samples were dissolved in $CDCl_3$ to record the spectrum. Data were analyzed using MestRe-Nova software.

Powder X-ray diffraction: Powder X-ray diffraction was measured by a D8 Advance Bruker instrument using Cu Kα as the X-ray source (hν = 8047.8 eV).

Thermogravimetric analysis: Thermogravimetric measurements were performed using NETZSCH STA 449 F3 Jupiter TGA instrument equipped with Proteus-6.1.0 software. 4.82 mg Ag_{31} powder was used for the measurement. The study was performed in a temperature range of 30 to 800 °C under an argon atmosphere (gas flow rate 20 mL/min) with a heating rate of 10 °C/min.

For Ag_{31} cluster, TG measurement shows no significant mass losses upto 200 °C (shown in Figure 2c). Further heating leads to 27 % mass loss at 280 °C due to the detachments of six TRZ ligands and 46 % loss at 326 °C due to the dissociation of $[Ag_{11}S(TRZ)_2]$ fragment.

Electrochemical studies: The electrochemical behavior of the light-triggered conversion process of Ag_{31} cluster in DCM solution was studied using a CHI-600A potentiostat. 0.2 M tetrabutylammonium hexafluorophosphate (TBAF) solution was used as an electrolyte throughout the experiments. We have performed these experiments in a two-electrode setup, where a clean Pt wire (diameter 2 mm) acts as a working electrode and Ag/AgCl is used as a reference electrode. All the experiments were performed at room temperature (22 °C). Electrochemical photocurrent measurements in the solid state were performed in a three-electrode setup using a Bio-Logic SP-200 potentiostat. 3 mg cluster dissolved in 1 ml DCM was drop cast on a clean ITO glass slide (an active surface area of 1 cm^2) to prepare the working electrode. A platinum electrode (diameter 2 mm) was used as a counter electrode, and Ag/AgCl electrode acted as a reference electrode. 0.01 M Na_2SO_4 in water was used as an electrolytic solution for the photocurrent measurements. A white light source (xenon arc lamp) from Newport, India, was used as a white light source throughout the experiments.

TCSPC measurement: Time-resolved photoluminescence lifetime measurements were performed using a HORIBA Delta flex TCSPC spectrometer. The instrument was coupled with a ps pulse diode laser (pulse width of 85 ps) with an excitation wavelength centered at 405 nm. A HORIBA PPD-850 detector was used to record the decay profile.

Femtosecond transient absorption studies: The femtosecond TA measurements were performed using an ultrafast short laser pulse (pulse width 120 fs) centered at 800 nm. The pulse was generated by spectra physics Maitai oscillator with a few hundred nJ energy. The output beam was sent to Ti: sapphire optical amplifier to produce high energy pulses (pulse energy 4 mJ, width 120 fs, repetition rate 1 kHz). The output beam is further split into two parts: the first high-energy beam produces the second harmonic using β-barium borate crystal. The obtained 400 nm pulses are used to excite the sample with an intensity of 250 μJ/cm^2. The second part of the beam was used to generate the white light continuum probe pulses (450-800 nm) by CaF_2 crystal. The computer-controlled motion controller creates the delay between pump and probe pulses. The absorbance changes in the probe beam are due to the pump being calculated using the equation-

$$\Delta A = \log\left[I_{ex}(s)/I_0(s)\right] - \left[I_{ex}(r)/I_0(r)\right]$$

Where, r and s correspond to the reference and sample, I_{ex} and I_o are transmitted intensities of probe pulse after excitation and in the ground state, respectively. The intensity of the transmitted pulse is measured with the help of MS 2004.

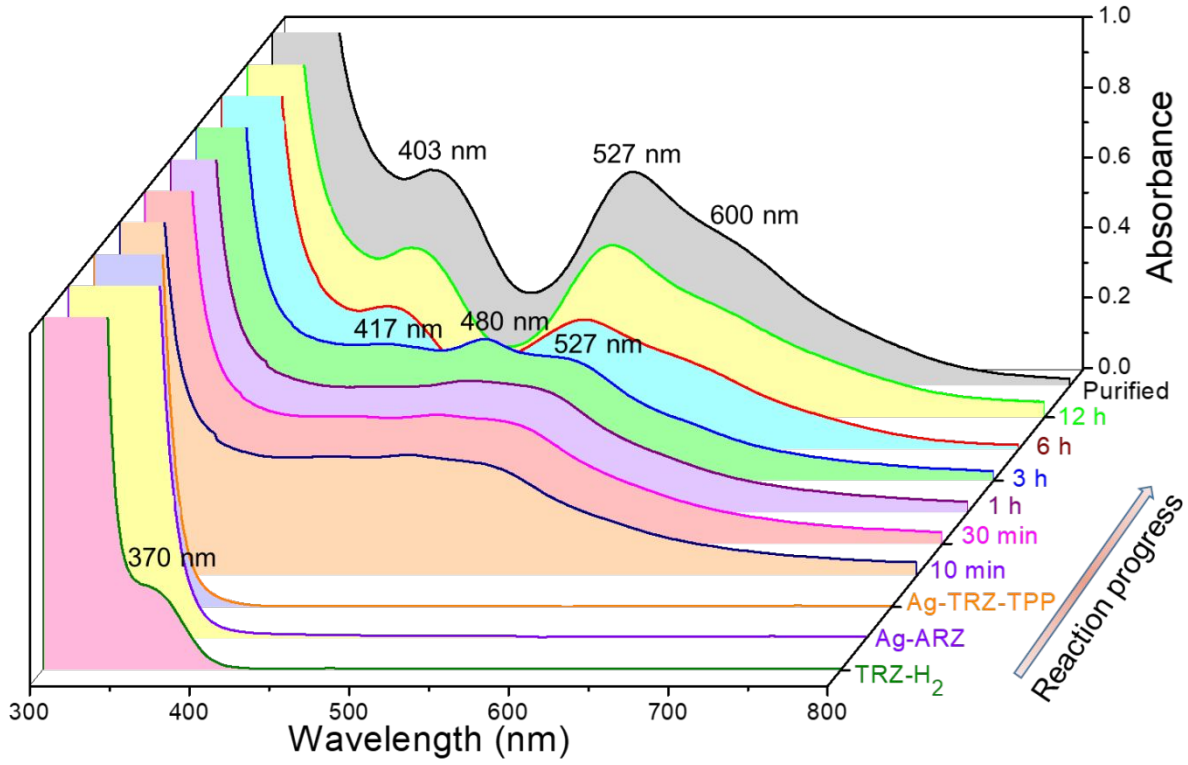

Figure S1. Time-dependent UV-vis absorption spectra show the formation of Ag_{31} cluster during the progression of TPP-assisted metal-thiolate reduction reaction.

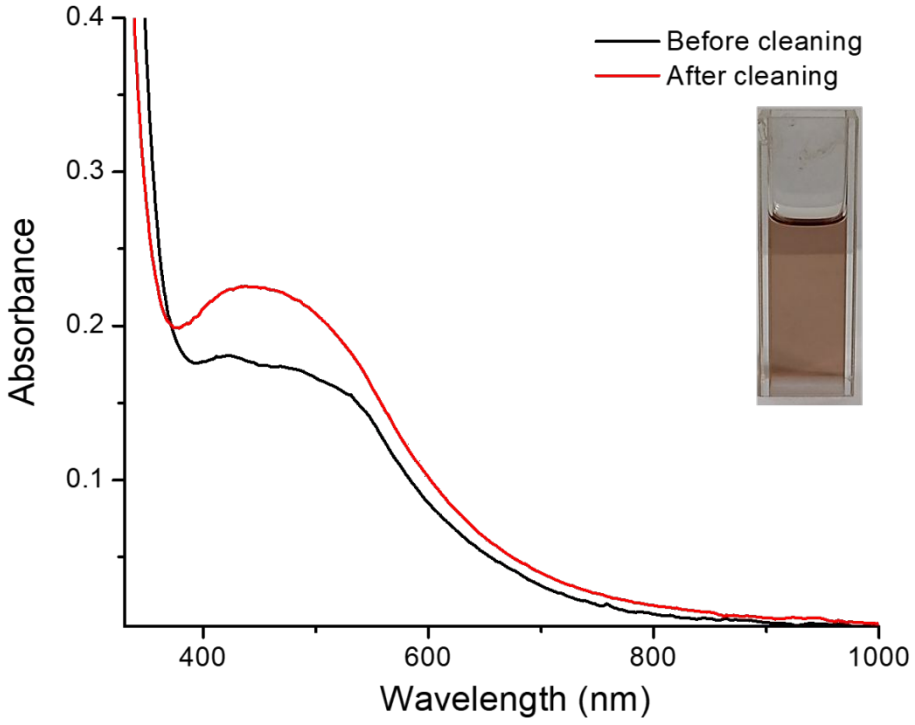

Figure S2. UV-vis absorption spectra of the product formed without TPP. All other precursors and reaction conditions are similar for the synthesis. Inset shows a photograph of the product in DCM.

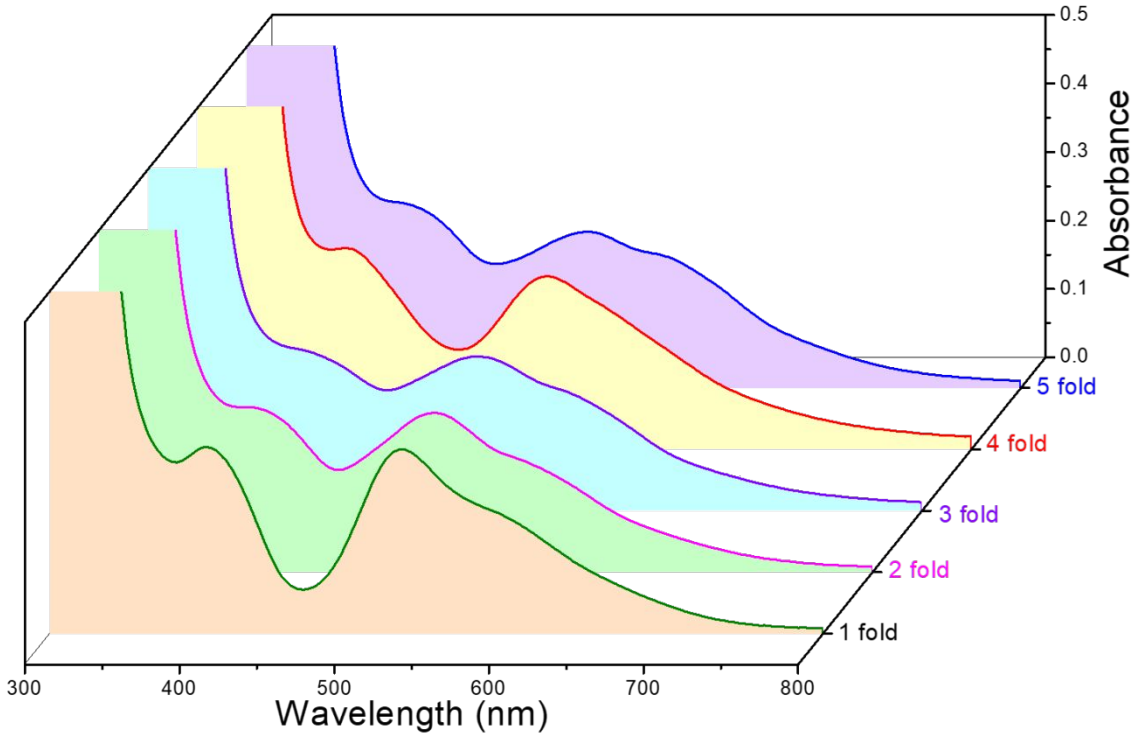

Figure S3. Nearly identical UV-vis absorption spectra show a five-fold scale-up of the synthesis of Ag_{31} using TPP-assisted metal thiolate reduction reaction.

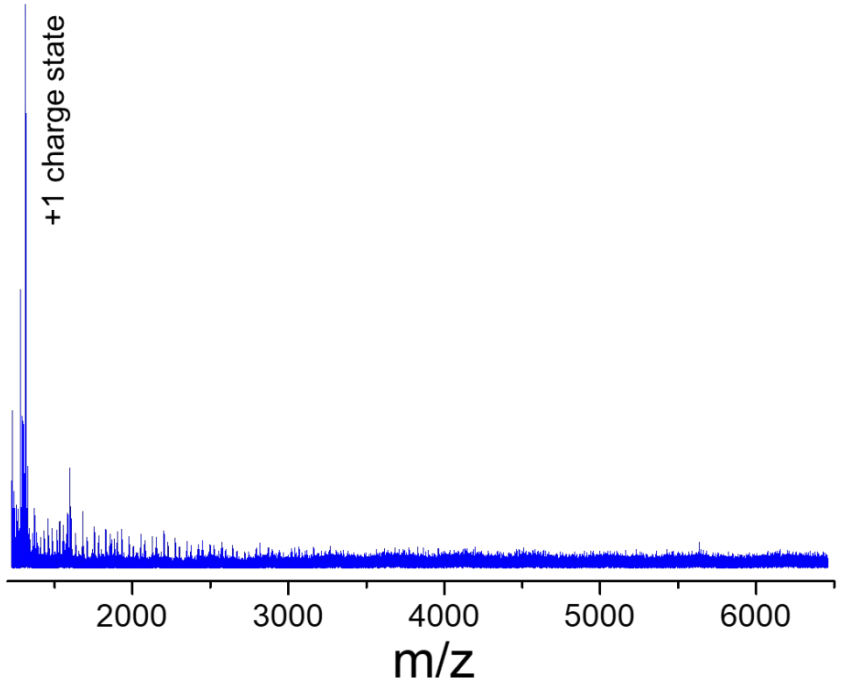

Figure S4. The positive ion mode ESI-MS spectrum of the as prepared Ag_{31} shows no prominent peaks in the spectrum.

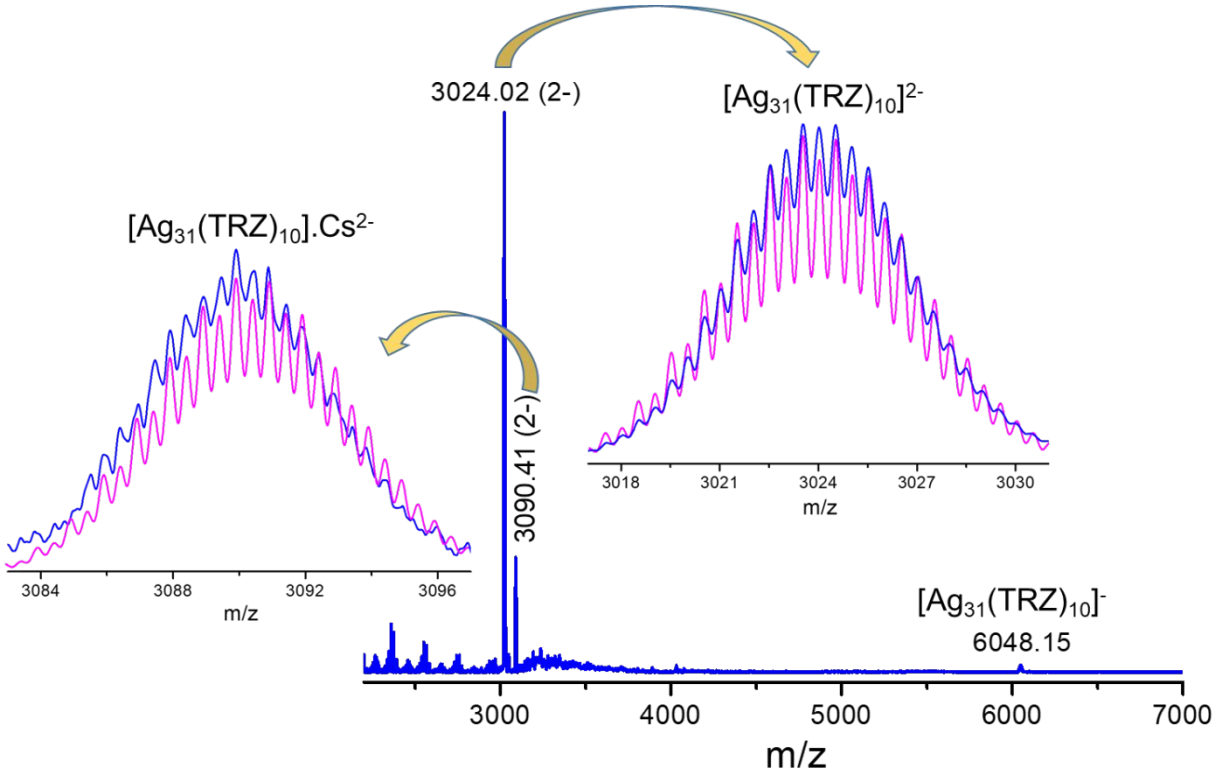

Figure S5. Negative ion mode ESI-MS spectrum of Ag_{31} nanocluster after the addition of cesium acetate. The inset depicts a comparison of the isotopic distribution of the experimental and theoretical spectra.

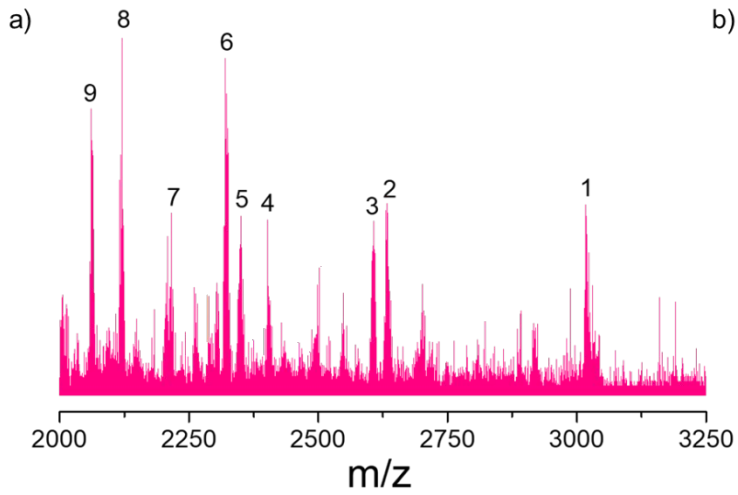

b)

Peak No.	Mass	Composition
1	3019.84	$[Ag_{14}S_5(TRZ)_5]^-$
2	2633.04	$[Ag_{11}S_3(TRZ)_5]^-$
3	2608.05	$[Ag_{14}S_9(TRZ)_3]^-$
4	2404.17	$[Ag_{13}S_6(TRZ)_3]^-$
5	2351.79	$[Ag_9S(TRZ)_5]^-$
6	2320.04	$[Ag_9(TRZ)_5]^-$
7	2213.09	$[Ag_8(TRZ)_5]^-$
8	2120.32	$[Ag_9S_2(TRZ)_4H_5]^-$
9	2061.42	$[Ag_{11}S_2(TRZ)_3]^-$

Figure S6. a) Expanded view of the higher mass range in the MS/MS spectrum of Ag_{31} at CE 60. b) Analysis of the molecular composition of the fragments.

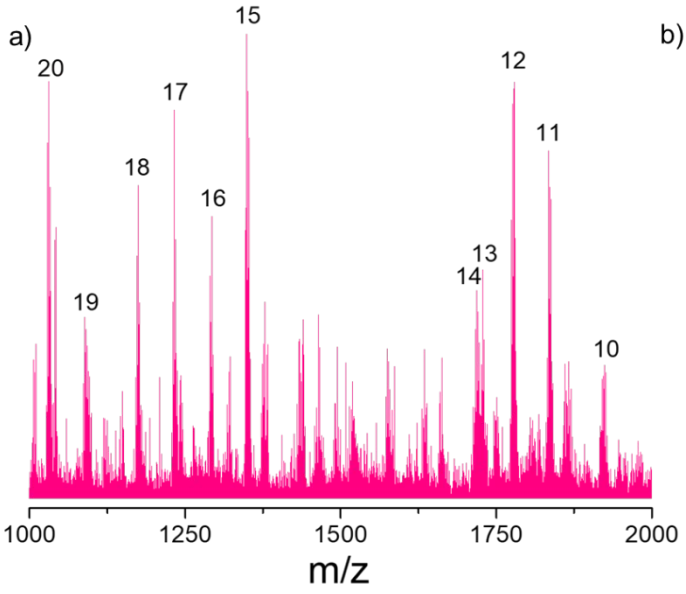

b)

Peak No.	Mass	Composition
10	1922.23	$[Ag_5S(TRZ)_5H]^-$
11	1836.29	$[Ag_{12}(TRZ)_2H_2]^-$
12	1779.93	$[Ag_9(TRZ)_3]^-$
13	1728.47	$[Ag_{11}(TRZ)_2H_2]^-$
14	1718.46	$[Ag_{10}S_3(TRZ)_2H_4]^-$
15	1350.52	$[Ag_5(TRZ)_3H]^-$
16	1292.64	$[Ag_8S_5(TRZ)]^-$
17	1232.74	$[Ag_8S_3(TRZ)H_4]^-$
18	1174.87	$[Ag_{10}S_3]^-$
19	1090.95	$[Ag_7S_2(TRZ)H_2]^-$
20	1031.01	$[Ag_7(TRZ)H_6]^-$

Figure S7. a) Expanded view of the lower mass range in the MS/MS spectrum of Ag_{31} at CE 60. b) Analysis of the molecular composition of the fragments.

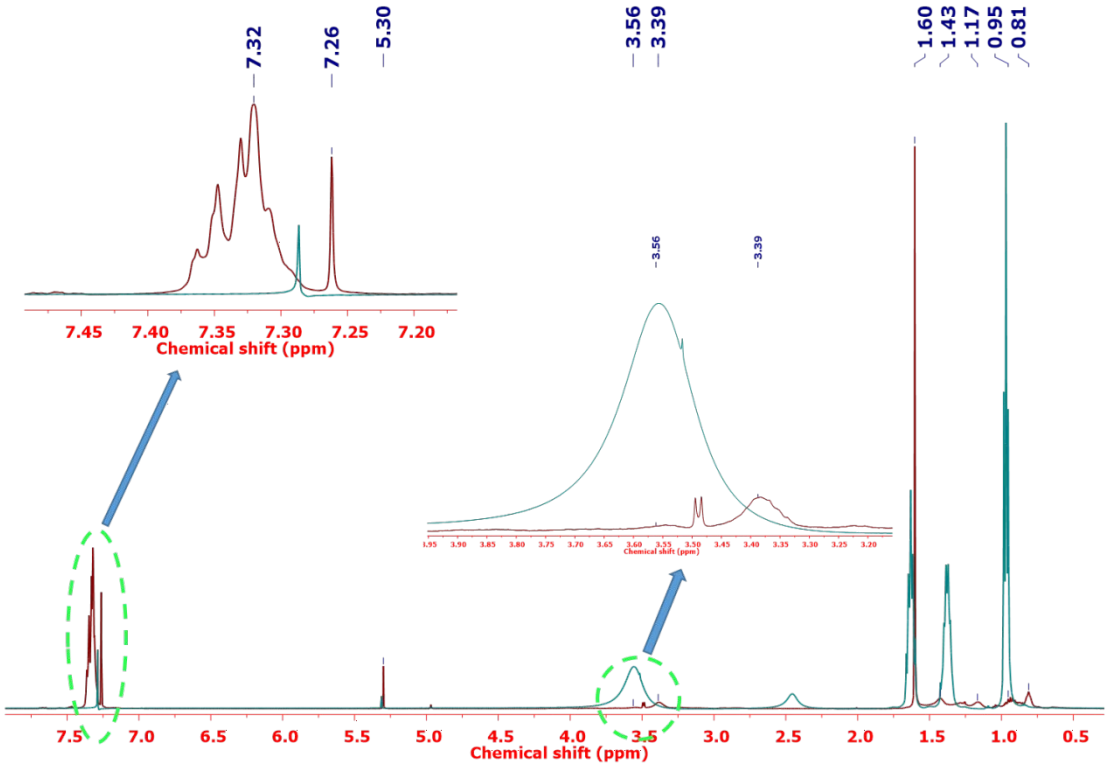

Figure S8. Full range ^1H NMR spectrum of Ag_{31} in comparison to TRZ-H_2 ligand. The trace impurity peak at 7.32 (m), 7.26 (s), 5.30 (s) ppm are due to TPP, $CHCl_3$ and dichloromethane, respectively. Color code: orange = Ag_{31} cluster, blue = TRZ-H_2 ligand.

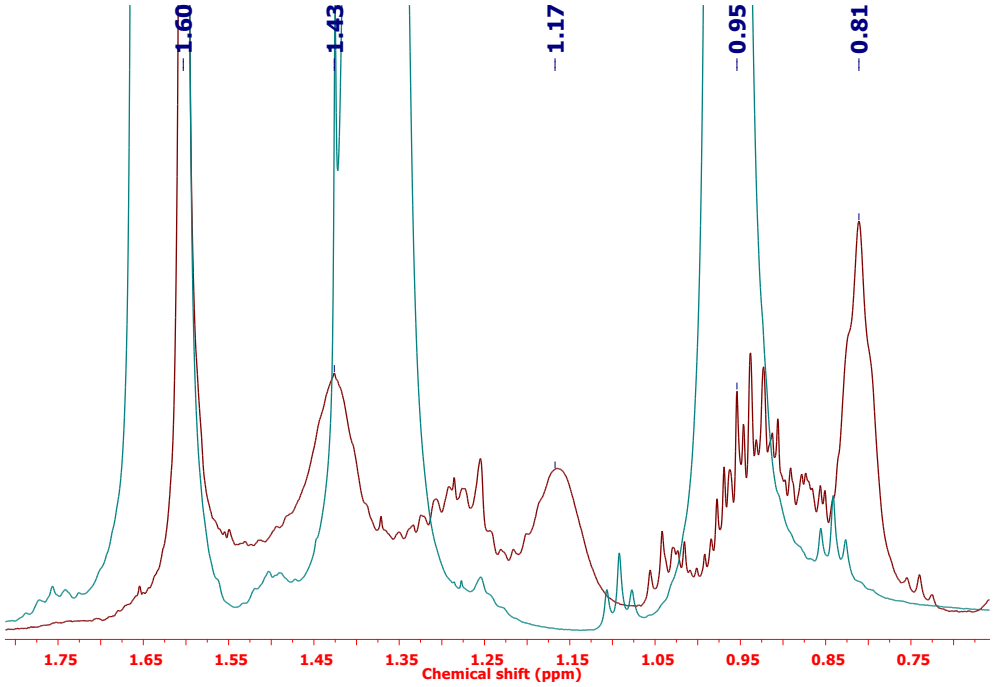

Figure S9. An expanded (0.5-1.75 ppm) ^{1}H NMR spectrum of Ag_{31} in comparison to TRZ-H_2 ligand. Color code: orange = Ag_{31}, blue = TRZ-H_2 ligand.

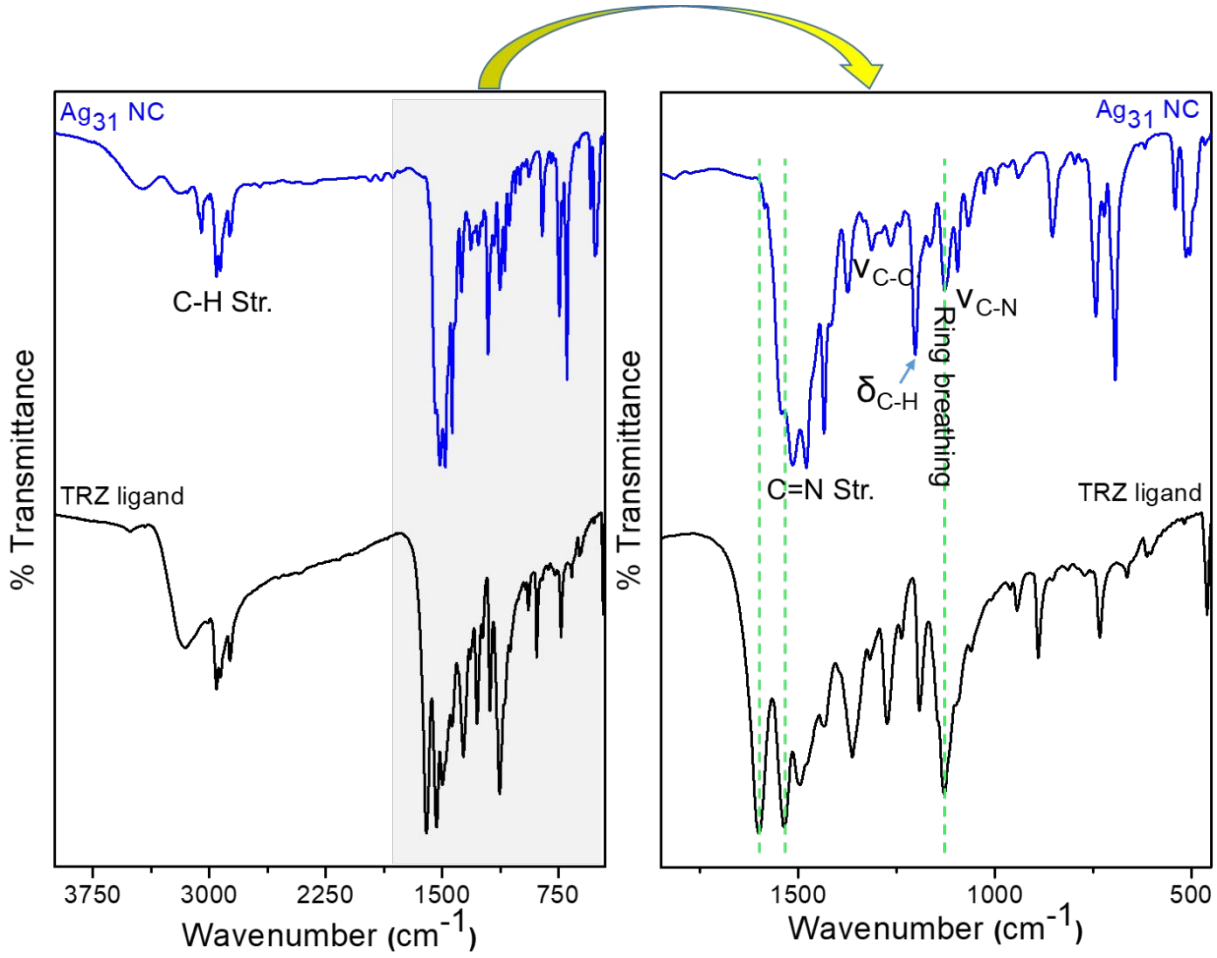

Figure S10. FT-IR spectra of Ag_{31} along with TRZ-H_2 ligand. Peaks of interest are marked.

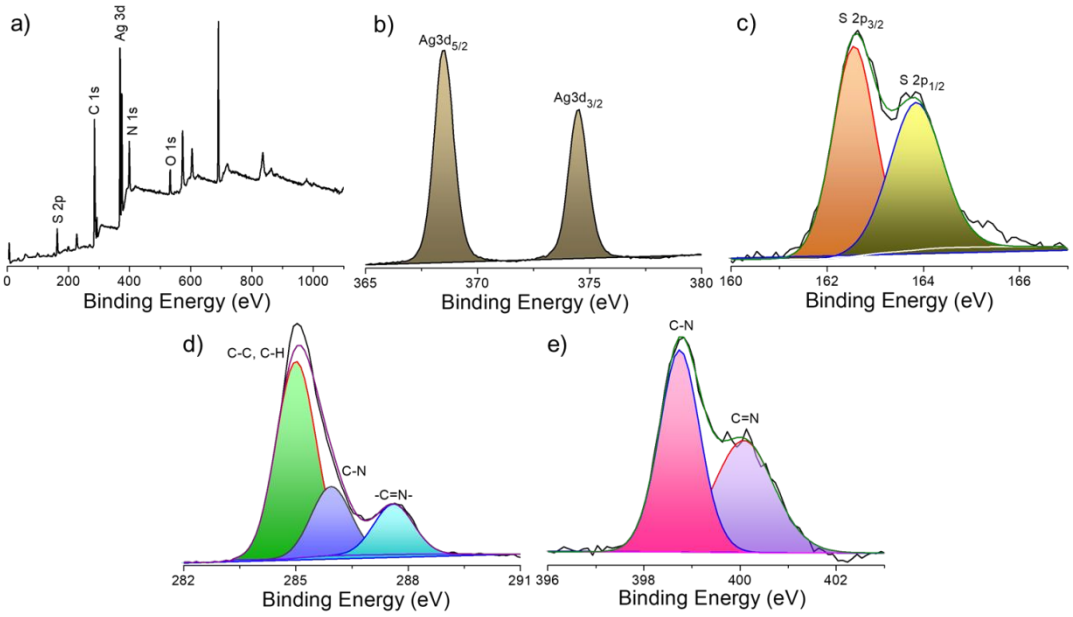

Figure S11. a) XPS survey spectrum of Ag_{31} shows the presence of expected elements. b-e) Selected area scans showed the respective elements. The binding energies of Ag $3d_{5/2}$ and $3d_{3/2}$ are 368.5 and 374.4 eV, respectively, indicative of metal-like Ag(0) states.[1,2] Spectral fittings of the C 1s region shows three binding energies at 285.0, 285.9, and 287.5 eV due to C-C, C-N, and C=N regions, respectively. We have also observed two fitted regions of N 1s at 398.7 and 400.0 eV for C-N and C=N bonding, respectively.[3]

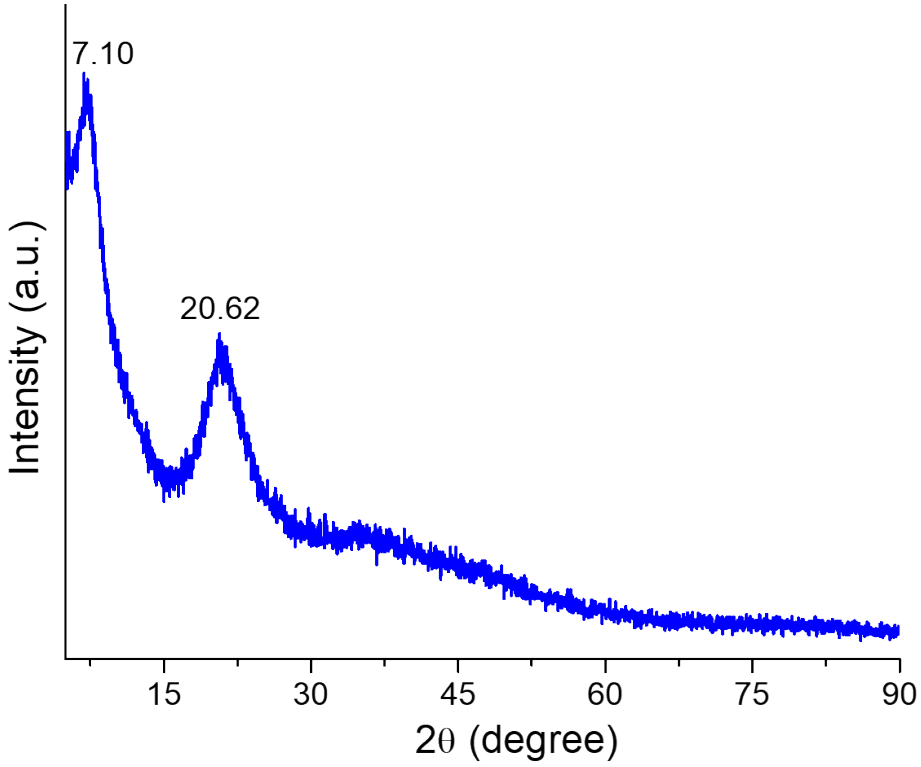

Figure S12. Powder X-ray diffraction spectrum of Ag_{31} shows weak diffraction peaks due to the lack of crystallinity.

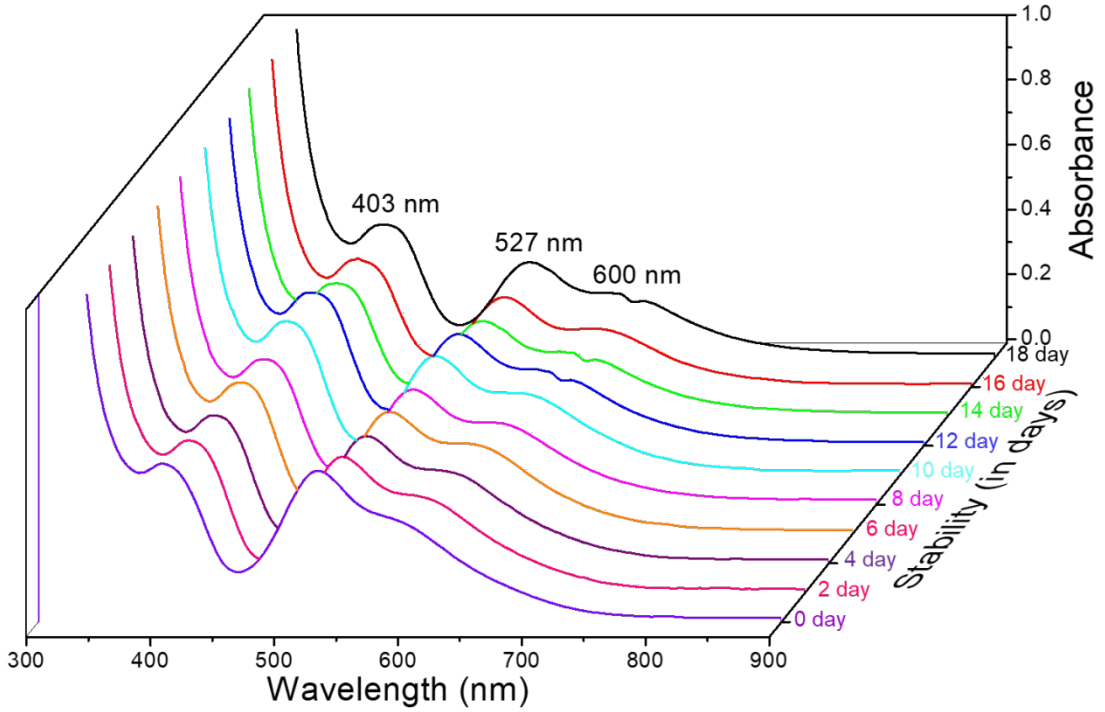

Figure S13. UV-vis absorption spectra with identical absorption features indicate the stability of Ag_{31} in $CHCl_3$ solution.

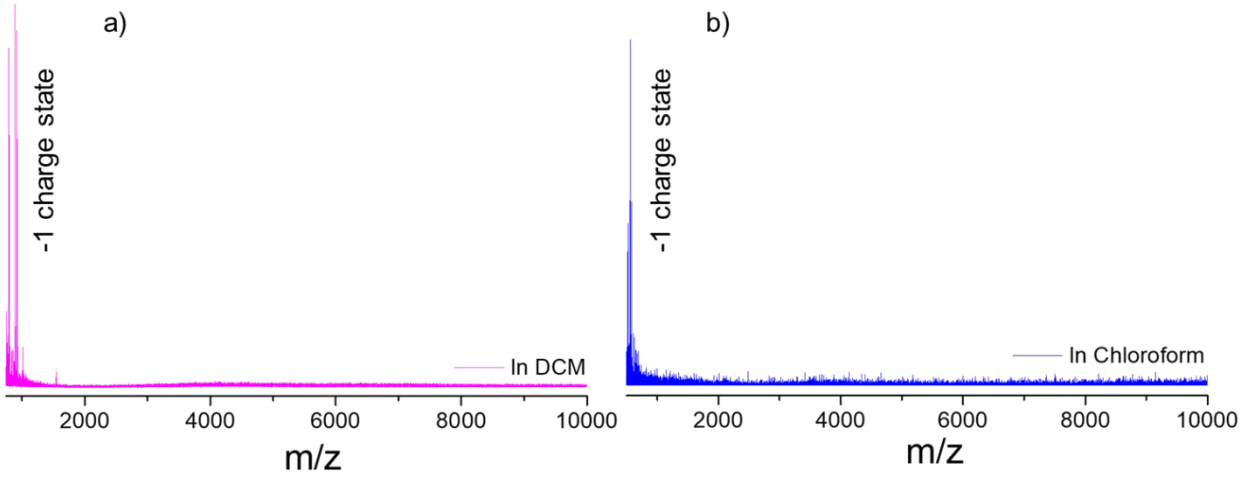

Figure S14. Mass spectra of light-triggered products in a) DCM and b) chloroform solvent in negative ion mode. Features of Ag_{31} and other clusters were not observed. Mononegative charge state peaks are due to complexes.

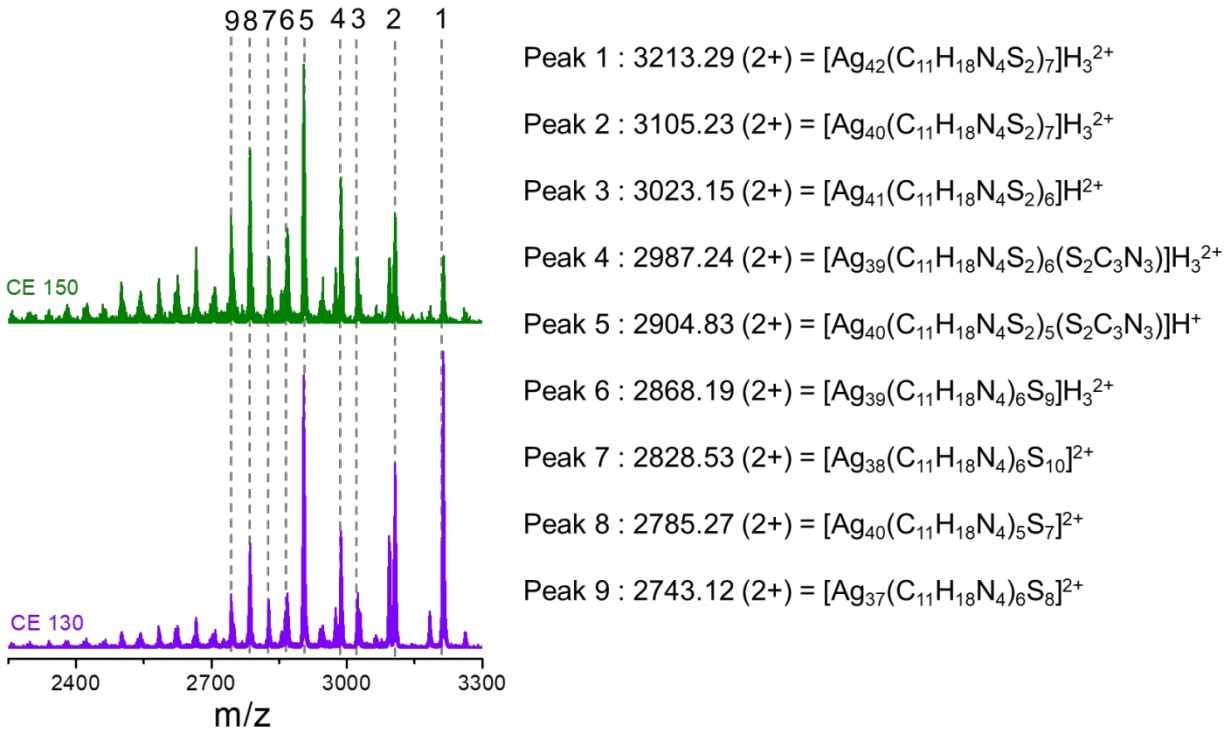

Figure S15. Expanded views of the lower range collision energy-dependent fragmentation spectra of Ag_{42}. Molecular composition of the respective ion peaks are shown here.

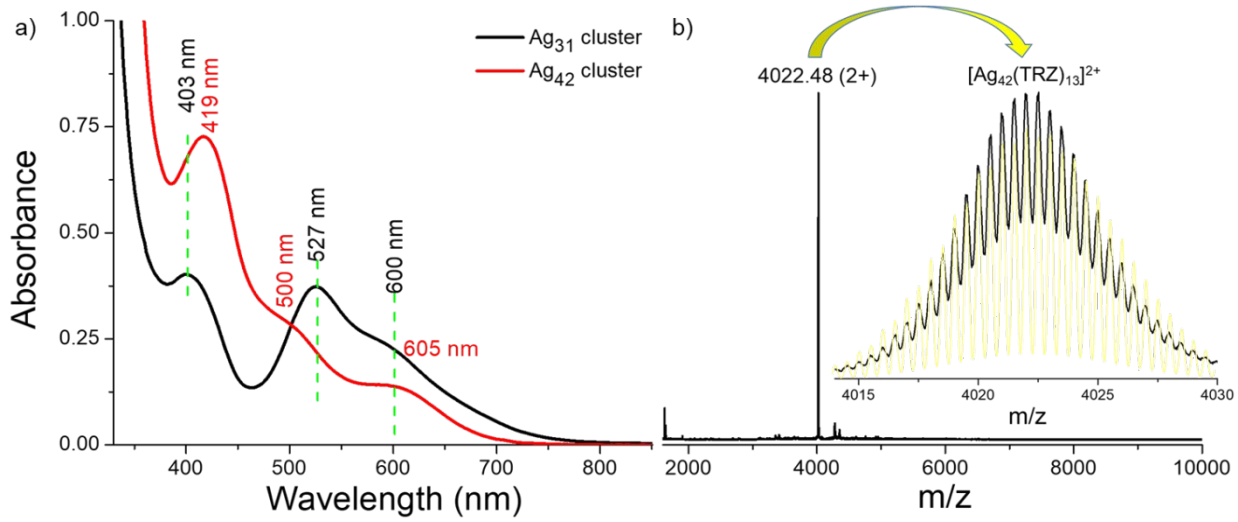

Figure S16. a) UV-vis absorption spectra shows the light-triggered interconversion of Ag_{31} dissolved in chloroform. b) ESI-MS data of the light-triggered product shows the formation of Ag_{42} nanocluster as a predominant end product. Inset shows the matching of the experimental (black) and theoretical (yellow) spectrum.

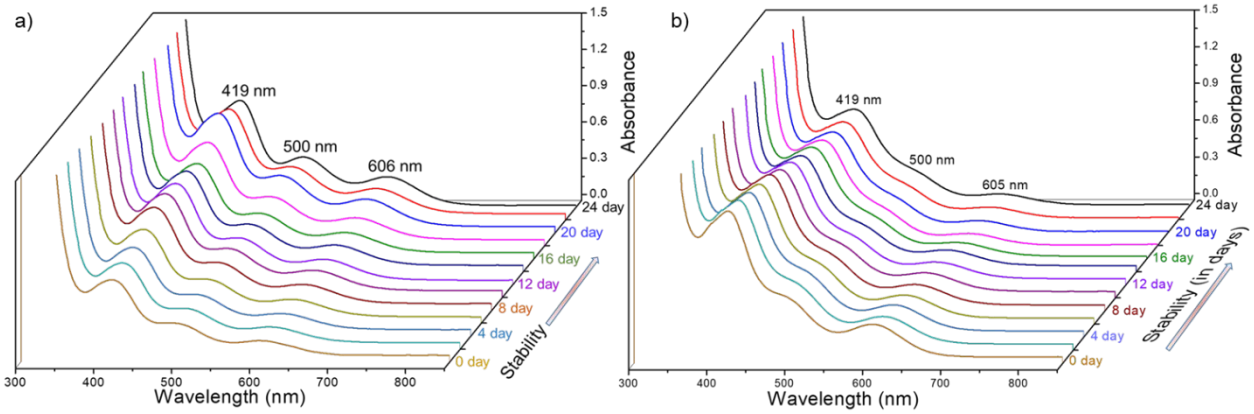

Figure S17. Time dependent UV-vis absorption spectra of Ag_{42} with identical spectral feature in a) DCM and b) chloroform, which demonstrated its stability.

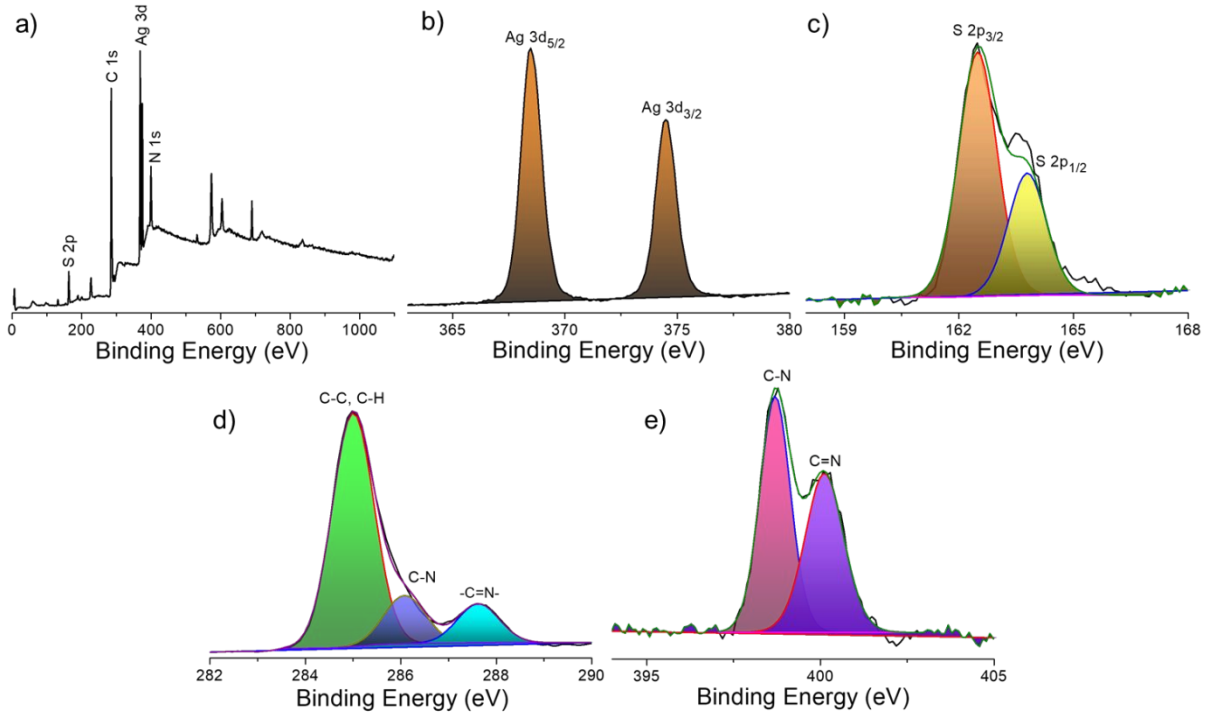

Figure S18. a) XPS survey scan of Ag_{42} indicating the presence of all the elements. Selected area spectral fittings of b) Ag 3d, c) S 2p, d) C 1s and e) N 1s regions.

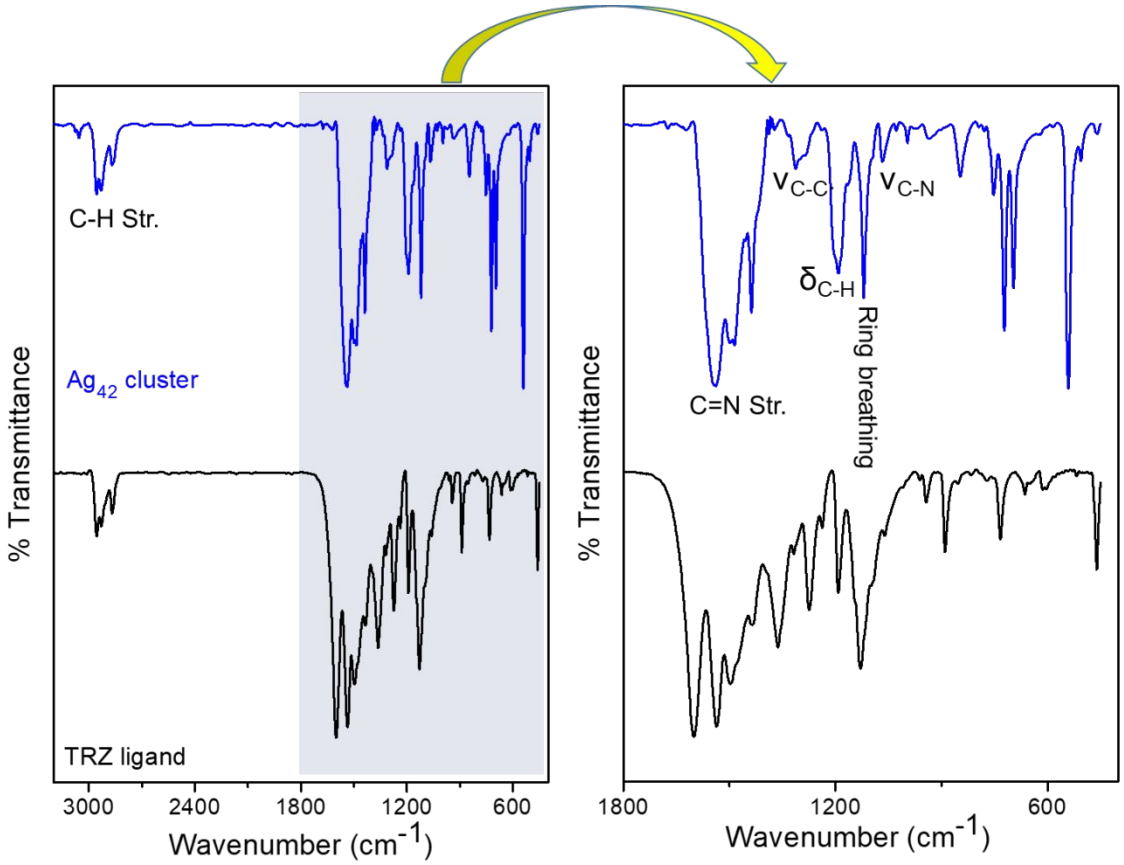

Figure S19. Comparative FT-IR spectra of Ag_{42} cluster and TRZ-H_2 ligand. Peaks of interest are marked.

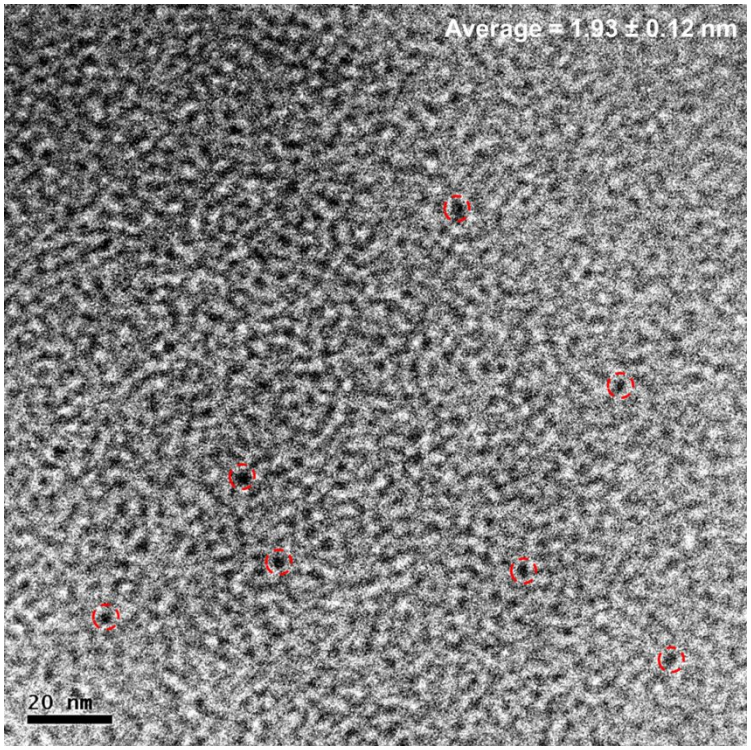

Figure S20. TEM micrograph of the Ag_{42} cluster. Ultrasmall cluster particles are marked in red.

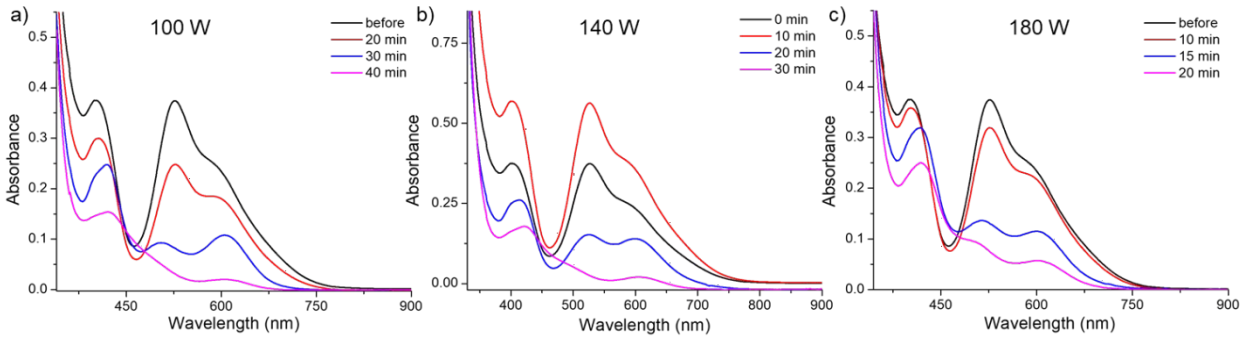

Figure S21. a-c) Lamp power-dependent conversion of Ag_{31} to Ag_{42} in its DCM solution. Cluster concentration was 1 mg/ml for each measurement.

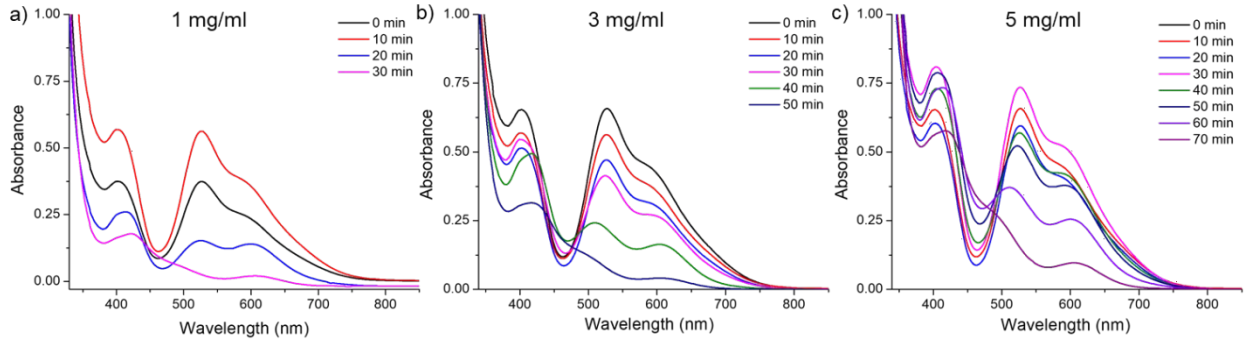

Figure S22. Concentration-dependent conversion of Ag_{31} to Ag_{42} in its DCM solution. Lamp power was 140 W for all the experiments.

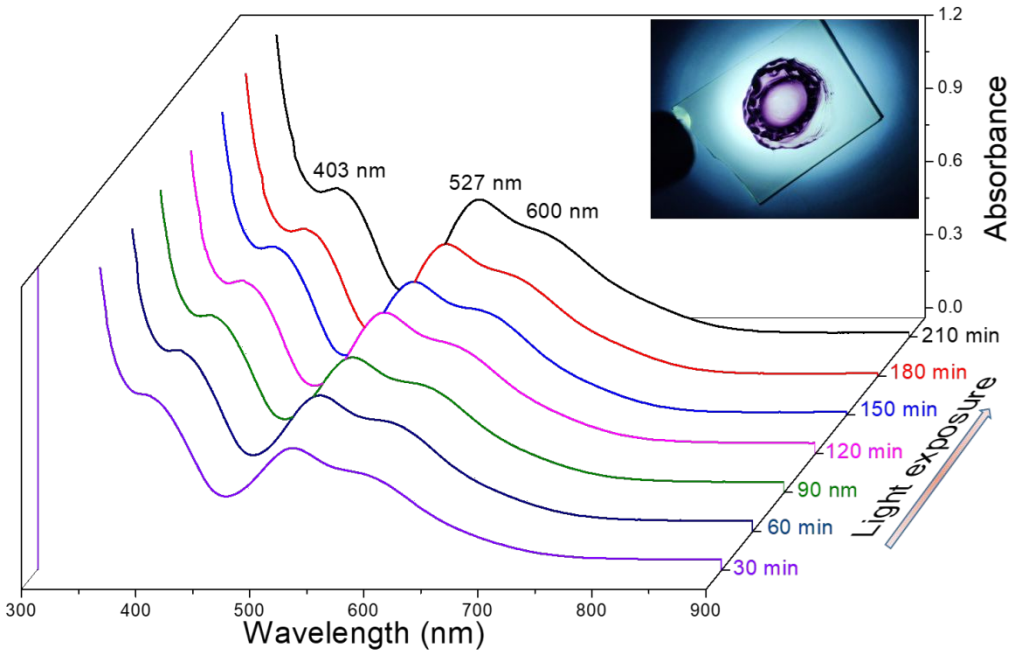

Figure S23. UV-vis absorption spectra of Ag_{31} after light irradiation in solid state. All the measurements were performed using a xenon arc lamp (lamp power = 140 W). Inset shows the photograph of a thin film during the process of light illumination.

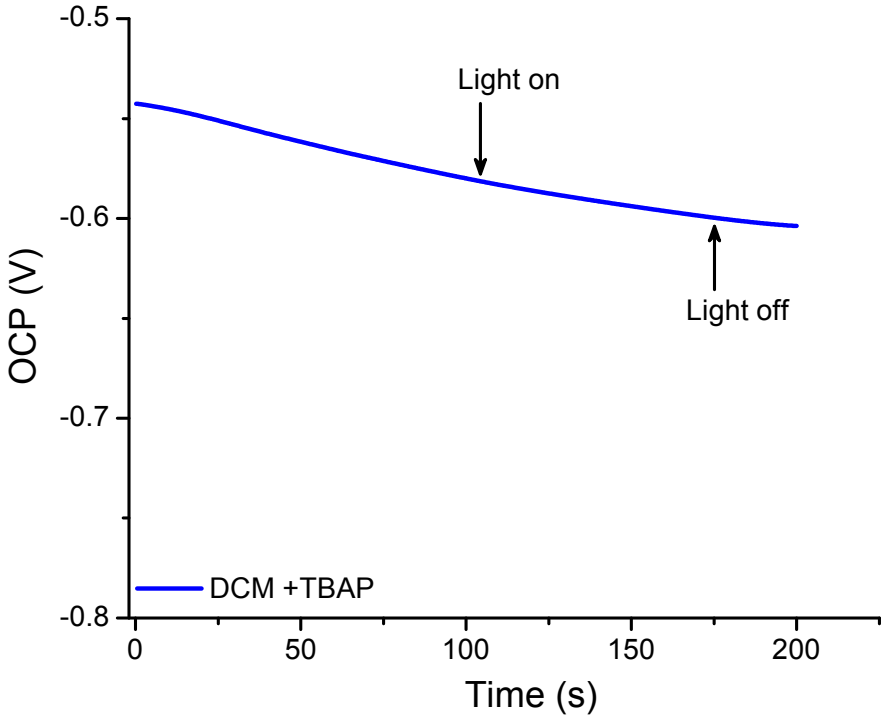

Figure S24. Open circuit potential (OCP) measurement of 0.2 M TBAF in DCM solution in dark and light illumination (140 W) using Pt wire as a working electrode and Ag/AgCl as reference electrode.

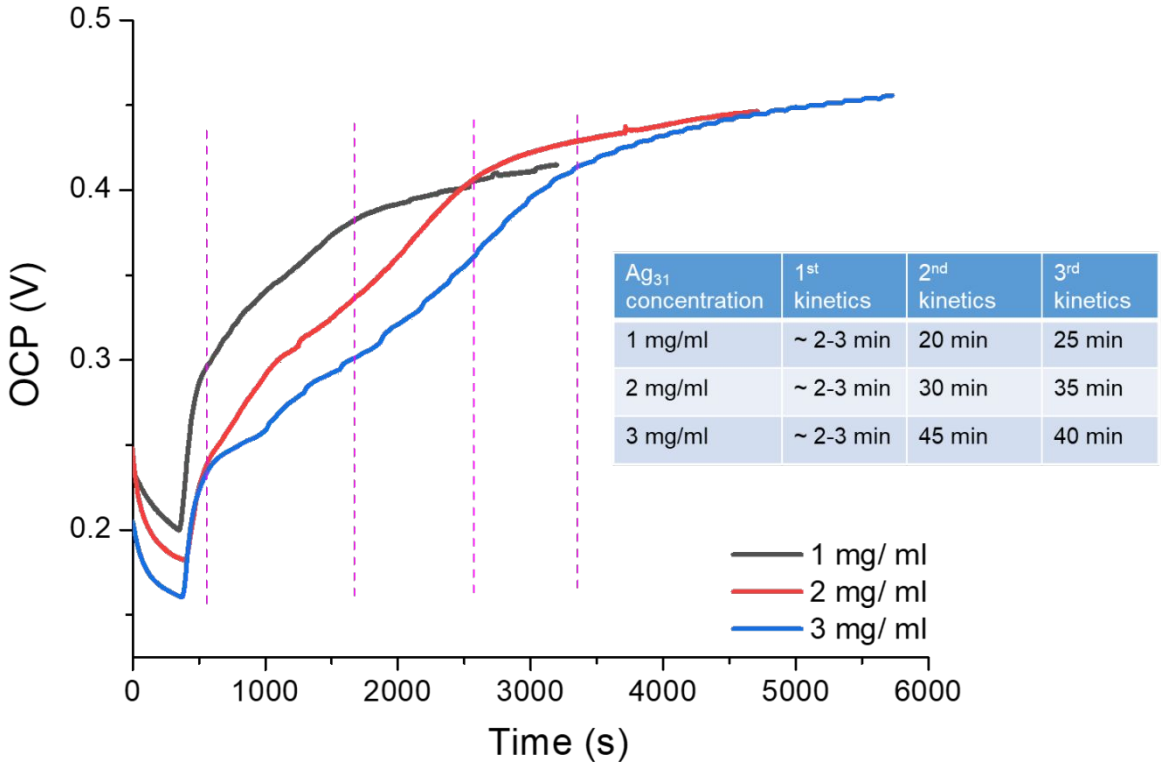

Ag_{31} concentration	1st kinetics	2nd kinetics	3rd kinetics
1 mg/ml	~ 2-3 min	20 min	25 min
2 mg/ml	~ 2-3 min	30 min	35 min
3 mg/ml	~ 2-3 min	45 min	40 min

Figure S25. Open circuit potential (OCP) measurements of Ag_{31} at different concentrations. Electrolyte used was 0.2 M TBAF in dichloromethane and lamp power was 140 W.

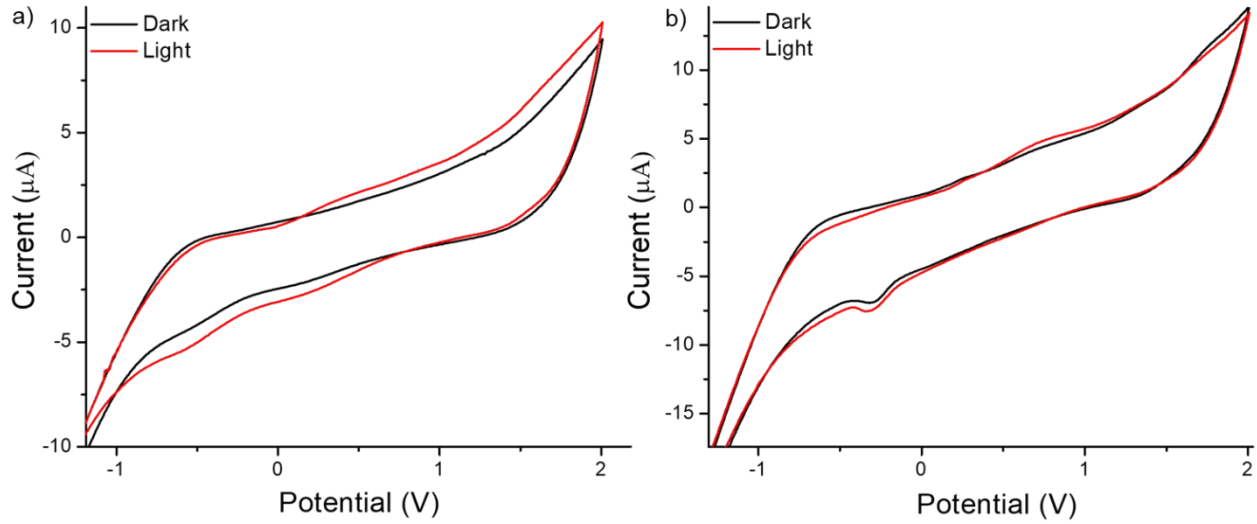

Figure S26. Cyclic voltammograms of a) Ag_{31}, b) Ag_{42} clusters before and after light irradiation (lamp power 140 W) in 0.2 M TBAF solution, in DCM.

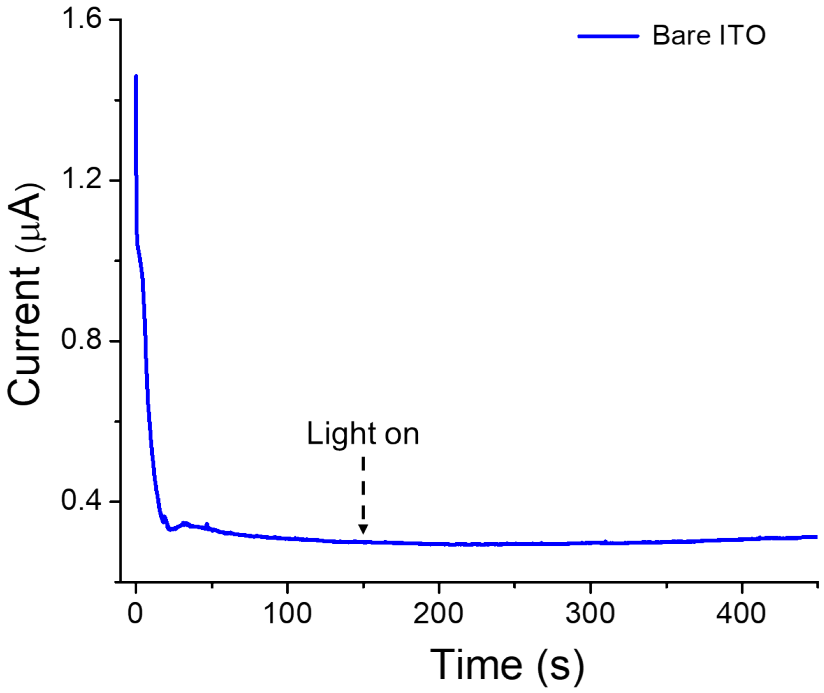

Figure S27. Chronoamperometric photocurrent response of a bare ITO electrode under electrochemical conditions (electrolyte used was 0.5 M aqueous Na_2SO_4, lamp power 140 W).

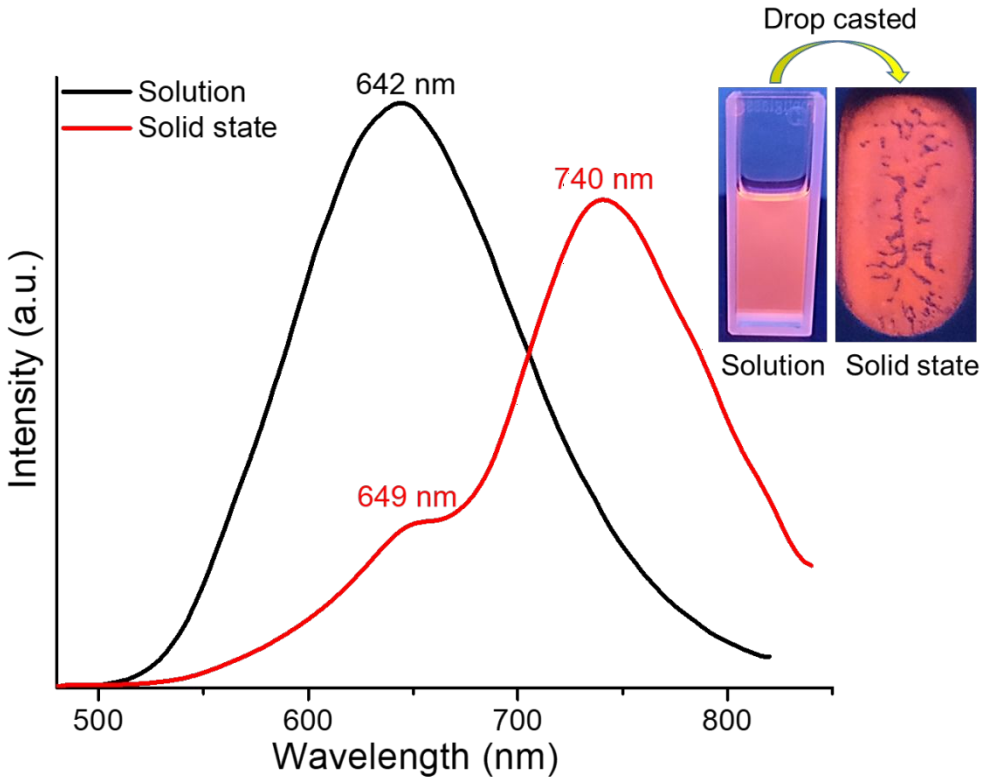

Figure S28. Comparative PL emission spectra of Ag_{42} nanocluster by 480 nm excitation in DCM solution as well as in the solid state. Inset showed the photographs of the respective clusters under 365 nm UV lamp.

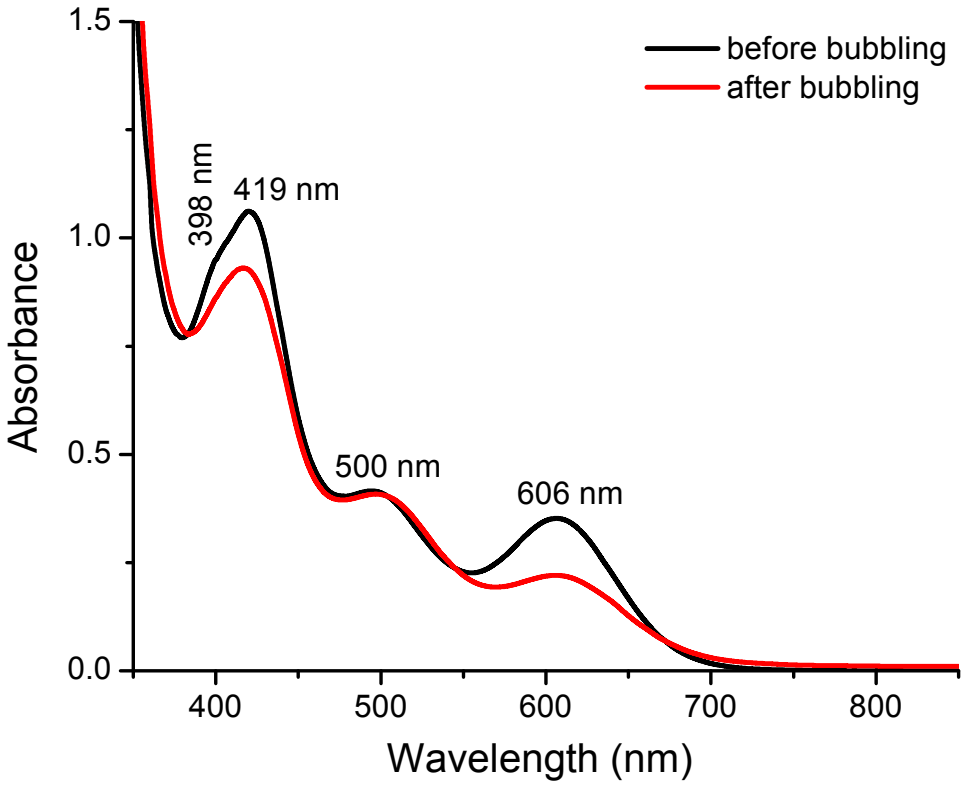

Figure S29. Comparative UV-vis absorption spectra of Ag_{42} in DCM solution before and after oxygen bubbling. Time of bubbling was 30-35 min.

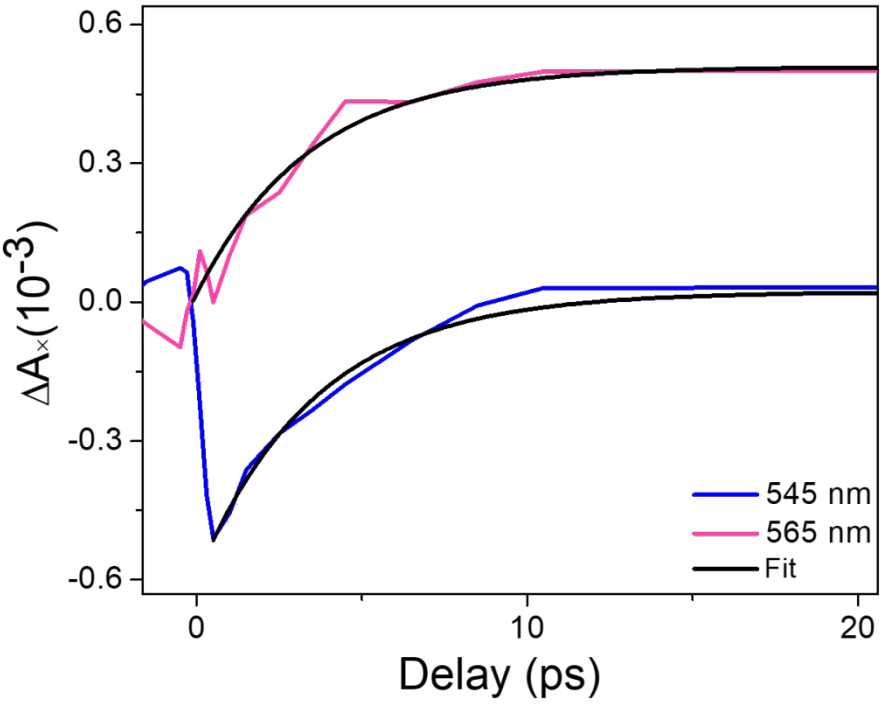

Figure S30. Early time scale temporal spectral profiles with associated fittings for Ag_{31} nanocluster.

References:

(1) Wagstaffe, M.; Hussain, H.; Acres, M. J.; Jones, R.; Syres, K. L.; Thomas, A. G. Structure and Reactivity of a Model Oxide Supported Silver Nanocluster Catalyst Studied by near Ambient Pressure X-Ray Photoelectron Spectroscopy. *J. Phys. Chem. C* **2017**, *121* (39), 21383–21389.

(2) Yang, L.; Jiang, X.; Ruan, W.; Yang, J.; Zhao, B.; Xu, W.; Lombardi, J. R. Charge-Transfer-Induced Surface-Enhanced Raman Scattering on Ag-TiO_2 Nanocomposites. *J. Phys. Chem. C* **2009**, *113* (36), 16226–16231.

(3) Chandra, S.; Sciortino, A.; Das, S.; Ahmed, F.; Jana, A.; Roy, J.; Li, D.; Liljeström, V.; Jiang, H.; Johansson, L.-S.; Chen, X.; Nonappa; Cannas, M.; Pradeep, T.; Peng, B.; Ras, R. H. A.; Sun, Z.; Ikkala, O.; Mess, F. Gold $Au(I)_6$ Clusters with Ligand-Derived Atomic Steric Locking: Multifunctional Optoelectrical Properties and Quantum Coherence. *Adv. Opt. Mater.* **2023**, *2202649*, 1–8.